ISSN 1070-3284, Russian Journal of Coordination Chemistry, 2024, Vol. 50, No. 1, pp. 49–60. © Pleiades Publishing, Ltd., 2024.

Redox-Active Tin(IV) Complexes Based on Sterically Hindered Catecholate Ligands

S. V. Baryshnikova[a], *, M. V. Arsen'ev[a], N. O. Druzhkov[a], G. K. Fukin[a], E. V. Baranov[a], and A. V. Piskunov[a]

[a] *Razuvaev Institute of Organometallic Chemistry, Russian Academy of Sciences, Nizhny Novgorod, Russia*

**e-mail: baryshnikova@iomc.ras.ru*

Received April 28, 2023; revised May 17, 2023; accepted May 19, 2023

Abstract—The oxidative addition of sterically hindered 3,6-dicyclohexyl-*o*-benzoquinone (L^1), 3,5-di-*tert*-octyl-*o*-benzoquinone (L^2), 4-*tert*-octyl-*o*-benzoquinone (L^3), and 3,5-bis(2-phenylpropyl)-*o*-benzoquinone (L^4) to tin(II) chloride in THF affords the corresponding tin(IV) catecholate complexes with the general formula $RCatSnCl_2 \cdot 2THF$, where Cat is the catecholate fragment; and R is 3,6-*c*-Hex (**I**), 3,5-*tert*-Oct (**II**), 4-*tert*-Oct (**III**), and 3,5-$C(Me)_2Ph$ (**IV**), regardless of the molar ratio of the starting reactants. The molecular structures of substituted *o*-benzoquinone L^4 and complexes **I** and **III** in the crystalline form are determined by X-ray diffraction (XRD) (CIF files CCDC nos. 2259370 (L^4), 2259371 (**I**), and 2259372 (**III**)). The oxidation–reduction properties of synthesized compounds **I**–**IV** are studied by cyclic voltammetry.

Keywords: catecholate, *o*-benzoquinone, tin(IV), cyclic voltammetry, XRD

DOI: 10.1134/S1070328423600778

INTRODUCTION

In several recent decades, the actively developed area of coordination chemistry that studies transition and nontransition metal complexes based on redox-active ligands attracts rapt attention of researchers in the fields of both fundamental and applied science [1–11]. Interest in these compounds is mainly caused by the fact that the redox-active ligands, being in the coordination sphere of the metal, are capable of reversible oxidizing and reducing to form radical-anion or dianionic species.

This specific feature made it possible to reveal many interesting peculiarities and unusual properties of compounds of this class. Among them are metallotropy and elementotropy, a unique sensitivity of EPR spectral parameters of the *o*-semiquinone and *o*-iminosemiquinone complexes to the nature and solvating ability of the solvent [12], intramolecular redox isomerism and a phenomenon of photo-/thermomechanical effect (reversible bending of crystals of the complex under the action of radiation or heat) [13–15], intramolecular electron transfer induced by the substitution of neutral ligands in the coordination sphere of the metal [16], and unusual magnetic properties caused by different types of metal–paramagnetic ligand and ligand–ligand magnetic interactions [1, 17, 18]. The predominant majority of the compounds demonstrating the above listed nontrivial properties refers to transition metal derivatives, and the processes themselves are accompanied by a change in the oxidation state of the transition metal. Unlike transition metals, nontransition metals have no multiple stable oxidation states. Under certain conditions, a combination of the nontransition metal and redox-active ligand in one molecule makes it possible to model the chemical behavior of the transition metal complexes. These compounds can participate in such processes as oxidative addition and reductive elimination. For example, unique phenomena of reversible binding of molecular oxygen [19, 20], oxidative addition of alkyl halides [21–23], and reversible addition of phenylacetylene to the nontransition metal complexes [24] have been discovered for the first time. It was also found that monocatecholate complexes of the main group metals can be oxidized with both nitrogen monoxide and dioxide to form the mono-*o*-benzosemiquinone derivatives [25, 26]. Thus, depending on the ligand nature, the catecholate complexes of nontransition metals can change their oxidation–reduction properties, which allows the boundaries of redox transformation to be extended to a significant extent and make them promising from the viewpoint of development of the chemistry of the main group metals with redox-active ligands as a boundary range

between the chemistry of transition and nontransition metal complexes.

In this work, new sterically hindered *o*-benzoquinone and a series of redox-active tin(IV) complexes with sterically hindered catechols were synthesized, their molecular structures were determined, and the electrochemical properties were studied.

EXPERIMENTAL

All procedures on the synthesis of the tin complexes with substituted *o*-benzoquinones were carried out without air oxygen and moisture. The solvents used in the syntheses were purified and dehydrated according to published recommendations [27, 28]. *o*-Benzoquinones L^1–L^3 were synthesized using a known procedure [29, 30]. ^{1}H NMR spectra were recorded on a Bruker Avance Neo (300 MHz) spectrometer. For NMR spectra recording, $CDCl_3$ was used as the solvent. IR spectra in a range of 400–4000 cm^{-1} were recorded on an FSM-1201 FT-IR spectrometer in Nujol. Elemental analysis was carried out on an Elementar Vario EL cube elemental analyzer. Electrochemical measurements were conducted in a standard three-electrode cell in a CH_2Cl_2 solution using a Smartstat PS-50 potentiostat. A glassy carbon disk electrode (d = 2 mm) served as the working electrode. A platinum wire and Ag/AgCl/KCl (sat.) were used as the auxiliary electrode and reference electrode, respectively. All measurements were carried out in an argon atmosphere. The scanning rate was 200 mV/s, and n-Bu_4NClO_4 (0.2 M) served as the electrolyte. The concentration of the complexes was 2×10^{-3} mol/L.

Synthesis of 3,5-bis(2-phenylpropan-2-yl)-*o*-benzoquinone (L^4). A mixture of pyrocatechol (2.2 g, 0.02 mol), α-methylstyrene (7.08 g, 0.06 mol), and titanium bis(catecholate) (0.3 g) was heated at 160°C for 6 h. Then an α-methylstyrene excess was removed under reduced pressure, and the reaction mixture was dissolved in $CH_3C(O)OH$ (20 mL) and oxidized by the dropwise addition of concentrated HNO_3 until NO_2 stopped to evolve. The product was extracted with hot hexane, washed with water, and recrystallized from methanol. The yield of green crystals suitable for XRD was 2.34 g (34%).

For $C_{24}H_{24}O_2$		
Anal. calcd., %	C, 83.69	H, 7.02
Found, %	C, 83.85	H, 6.12

IR (Nujol, cm^{-1}): 1664 s, 1662 m, 1599 m, 1567 m, 1493 s, 1466 s, 1443 s, 1367 s, 1316 w, 1265 s, 1234 m, 1207 m, 1189 m, 1156 m, 1142 m, 1101 m, 1077 m, 1055 m, 1026 s, 1004 m, 988 w, 965 s, 941 m, 926 w, 913 m, 904 m, 879 s, 846 s, 805 s, 768 s, 704 s, 660 m, 614 m, 599 m, 573 s, 536 s, 502 m, 479 m.

^{1}H NMR ($CDCl_3$; δ, ppm): 1.40 (s, 6H, $2CH_3$), 1.57 (s, 6H, $2CH_3$), 6.41 (d, ^4J(HH) = 2.2 Hz, 1H, CH_{arom}), 6.46 (d, ^4J(HH) = 2.2 Hz, 1H, CH_{arom}), 7.00–7.45 (m, 10H, 2Ph). ^{13}C NMR ($CDCl_3$; δ, ppm): 27.16, 28.27, 42.02, 44.20, 122.82, 125.47, 125.97, 126.37, 127.26, 128.23, 128.97, 136.16, 144.38, 146.83, 148.56.

General procedure for the synthesis of complexes I–IV based on substituted *o*-benzoquinones. A solution of substituted *o*-benzoquinone (1 equiv) in THF (10 mL) was added to a solution of $SnCl_2$·dioxane (1 equiv) in the same solvent (20 mL). The color of the reaction mixture changed from green to yellow or brown. THF was evaporated under reduced pressure to dryness, and the residue was dissolved in a CH_2Cl_2–hexane (1 : 1) mixture. The tin(IV) complexes were isolated as finely crystalline yellow precipitates after the solution was hold at −18°C overnight. The crystals of complexes **I** and **III** suitable for XRD were obtained. All synthesized tin catecholate complexes **I**–**IV** were sensitive to air oxygen and moisture in the solution and solid state.

(3,6-*c*-HexCat)$SnCl_2$·2THF (I). A finely crystalline yellow precipitate was derived from ligand L^1 (0.250 g, 0.918 mmol) and $SnCl_2$·dioxane (0.254 g, 0.918 mmol). The yield was 0.523 g (94%).

For $C_{26}H_{40}O_4Cl_2Sn$		
Anal. calcd., %	C, 51.51	H, 6.65
Found, %	C, 51.76	H, 6.84

IR (Nujol; ν, cm^{-1}): 1456 s, 1414 m, 1377 m, 1364 m, 1325 w, 1276 s, 1252 s, 1178 w, 1137 m, 1075 s, 1053 w, 1024 w, 978 s, 955 s, 918 w, 893 m, 848 w, 816 s, 801 m, 742 s, 654 s, 602 s, 525 s.

^{1}H NMR ($CDCl_3$; δ, ppm): 0.71–1.53 and 1.60–2.07 (m, both 5H, $CH_{2cyclohex}$), 1.86 (m, 4H, $2CH_2$(THF)), 2.61–2.79 (m, 1H, $CH_{cyclohex}$), 3.83 (m, 4H, $2CH_2O$(THF)), 6.71 (s, 1H, CH_{arom}).

(3,5-*tert*-OctCat)$SnCl_2$·2THF (II). A finely crystalline brown precipitate was derived from ligand L^2

(0.250 g, 0.751 mmol) and $SnCl_2$·dioxane (0.208 g, 0.751 mmol). The yield was 0.461 g (92%).

For $C_{30}H_{52}Cl_2O_4Sn$		
Anal. calcd., %	C, 54.07	H, 7.87
Found, %	C, 54.36	H, 7.98

IR (Nujol; ν, cm^{-1}): 1567 s, 1465 m, 1416 s, 1395 m, 1378 m, 1363 s, 1349 m, 1333 m, 1300 m, 1289 m, 1253 s, 1234 s, 1213 w, 1182 w, 1134 m, 1103 w, 1043 w, 1002 s, 984 s, 969 s, 924 m, 909 m, 886 w, 834 s, 772 s, 741 m, 702 s, 680 w, 665 m, 637 m, 596 s, 525 s, 502 s.

^{1}H NMR ($CDCl_3$; δ, ppm): 0.73 and 0.75 (s, both 9H, $3CH_3$), 1.30 and 1.43 (s, both 6H, $2CH_3$), 1.67 and 1.93 (s, both 2H, CH_2), 1.88 (m, 8H, $2CH_2$(THF)), 3.86 (m, 8H, $2CH_2O$(THF)), 6.52 and 6.62 (d, ^4J(H,H) = 2 Hz, both 1H, CH_{arom}).

(4-*tert*-OctCat)$SnCl_2$·2THF (III). A finely crystalline pale yellow precipitate was derived from ligand L^3 (0.117 g, 0.531 mmol) and $SnCl_2$·dioxane (0.147 g, 0.531 mmol). The yield was 0.273 g (93%).

For $C_{22}H_{36}Cl_2O_4Sn$		
Anal. calcd., %	C, 47.68	H, 6.55
Found, %	C, 47.81	H, 6.64

IR (Nujol; ν, cm^{-1}): 1577 w, 1465 m, 1415 s, 1378 m, 1365 s, 1348 m, 1313 m, 1254 s, 1205 m, 1129 m, 1115 m, 1082 w, 1043 s, 1005 s, 946 m, 933 w, 919 m, 902 w, 864 m, 838 s, 805 s, 723 m, 693 m, 660 s, 619 m, 572 w, 513 w.

^{1}H NMR ($CDCl_3$; δ, ppm): 0.71 (s, 9H, $3CH_3$), 1.30 (s, 6H, $2CH_3$), 1.94 (s, 2H, CH_2), 1.88 (m, 8H, $2CH_2$(THF)), 3.86 (m, 8H, $2CH_2O$(THF)), 6.56–7.11 (m, 3H, CH_{arom}).

(3,5-C(Me)$_2$Ph-Cat)$SnCl_2$·2THF (IV). A finely crystalline yellow precipitate was derived from ligand L^4 (0.250 g, 0.726 mmol) and $SnCl_2$·dioxane (0.201 g, 0.726 mmol). The yield was 0.458 g (93%).

For $C_{32}H_{40}Cl_2O_4Sn$		
Anal. calcd., %	C, 56.66	H, 5.94
Found, %	C, 56.95	H, 6.05

IR (Nujol; ν, cm^{-1}): 1597 w, 1572 m, 1465 m, 1420 s, 1378 s, 1298 s, 1279 s, 1242 m, 1230 w, 1202 m, 1182 w, 1154 w, 1114 w, 1074 w, 1030 m, 999 m, 977 s, 919 m, 904 m, 812 m, 857 m, 828 s, 815 s, 767 s, 747 m, 722 m, 700 s, 662 w, 639 m, 614 s, 587 m, 562 m, 547 m, 534 m, 489 m.

^{1}H NMR ($CDCl_3$; δ, ppm): 1.61 and 1.70 (s, both 3H, CH_3), 1.86 (m, 8H, $2CH_2$(THF)), 3.84 (m, 8H, $2CH_2O$(THF)), 6.73 and 6.88 (d, ^4J(HH) = 2 Hz, both 1H, CH_{arom}), 7.39–7.08 (m, 10H, $2C_6H_5$).

XRD of *o*-benzoquinone L^4 and complexes **I** and **III** were carried out on Agilent Xcalibur E (for L^4 and **IV**, T = 298(2) K) and Bruker D8 Quest (for **I** and **III**, T = 100(2) K) automated single-crystal diffractometers (ω and φ scan modes, MoK_α radiation, λ = 0.71073 Å). The collection of diffraction data, initial indexing of reflections, and refinement of unit cell parameters were performed using the CrysAlisPro [31] (for L^4) and APEX4 [32] (for **I** and **III**) programs. Experimental sets of intensities were integrated using the CrysAlisPro [31] (for L^4 and **IV**) and SAINT [33, 34] (for **I** and **III**) programs. The structures were solved by the dual-space method using the SHELXT program [35] and refined by full-matrix least squares for F^2_{hkl} in the anisotropic approximation for non-hydrogen atoms. Hydrogen atoms were placed in geometrically calculated positions and refined isotropically by the riding model with fixed thermal parameters (U_{iso}(H) = 1.5U_{eq}(C) for CH_3 groups and U_{iso}(H) = 1.2U_{eq}(C) for other groups). The structures of compounds L^4, **I**, and **III** were refined using the SHELXTL software [36, 37]. An absorption correction for L^4 was applied empirically using the SCALE3 ABSPACK algorithm [38]. Absorption corrections for compounds **I** and **III** were applied using the SADABS program [39]. In complex **I**, one *Cy* substituent of the catecholate ligand is disordered over two positions. Molecule **A** of complex **III** contains disordered fragments of coordinated THF molecules. The crystallographic data and XRD experimental and structure refinement parameters are given in Table 1.

The structures were deposited with the Cambridge Crystallographic Data Centre (CIF files CCDC nos. 2259370 (L^4), 2259371 (**I**), and 2259372 (**III**) available at ccdc.cam.ac.uk/structures).

One-point DFT calculations of the periodical 3D structures of compounds **I** and **III** were performed in the framework of the B3LYP exchange-correlation functional [40, 41] in the CRYSTAL17 program [42] using the DGDZVP all-electron basis set [43–46]. The coordinates of atoms for the one-point DFT calculation were taken from the routine XRD experimental data for compounds **I** and **III**. The contraction coefficient of the reciprocal space was established to be 4, which corresponds to 30 K-points in the irreduc-

Table 1. Crystallographic data and experimental and structure refinement parameters for compound L^4 and complexes **I** and **III**

Parameter	Value		
	L^4	**I**	**III**
Empirical formula	$C_{24}H_{24}O_2$	$C_{26}H_{40}O_4Cl_2Sn$	$C_{22}H_{36}O_4Cl_2Sn$
FW	344.43	606.17	554.10
Crystal system	Triclinic	Triclinic	Triclinic
Space group	$P\bar{1}$	$P\bar{1}$	$P\bar{1}$
T, K	298(2)	100(2)	100(2)
λ, Å	0.71073	0.71073	0.71073
a, Å	10.6231(2)	6.9833(5)	7.7893(6)
b, Å	11.2965(2)	10.7268(8)	12.9674(10)
c, Å	18.3795(2)	19.4323(14)	25.298(2)
α, deg	80.619(1)	100.432(2)	85.554(2)
β, deg	83.776(1)	100.0950(19)	88.569(2)
γ, deg	62.917(2)	104.8902(19)	74.870(2)
V, Å^3	1936.03(6)	1345.31(17)	2459.2(3)
Z	4	2	4
ρ_{calc}, g/cm^3	1.182	1.496	1.497
μ, mm^{-1}	0.074	1.177	1.280
F(000)	736	624	1136
Crystal sizes, mm	0.97 × 0.49 × 0.21	0.44 × 0.39 × 0.21	0.44 × 0.35 × 0.05
Scan range over θ, deg	3.23–28.00	2.02–25.68	2.21–28.00
Number of measured/independent reflections	32345/9319	56520/5112	81105/11866
R_{int}	0.0150	0.0426	0.0479
Number of independent reflections with $I > 2\sigma(I)$	7652	4795	10001
Number of refined parameters/restraints	477/0	315/12	553/32
R_1, wR_2 ($I > 2\sigma(I)$)	0.0430, 0.1146	0.0239 0.0552	0.0280, 0.0613
R_1, wR_2 (for all data)	0.0535, 0.1204	0.0271 0.0573	0.0403, 0.0651
$S(F^2)$	1.054	1.073	1.053
Residual electron density (max/min), e/Å^3	0.260/–0.157	0.385/–0.721	1.299/–0.676

ible Brillouin zone in which the Hamiltonian matrix was diagonalized.

The PLATON program (version 60119) [47] was applied for the generation of 35168 and 64284 Miller independent reflections *hkl* for compounds **I** and **III** with the inverse resolution to $s = 1.16$ Å^{-1}. The XFAC option of the CRYSTAL17 program was used to obtain a set of theoretical structural factors F_{hkl} from the electron density function determined by one-point calculations of the nonoptimized crystal structures of compounds **I** and **III**.

Based on the calculated structural amplitudes F_{hkl} using the MoPro program [48] in the framework of the Hansen–Coppens multipole formalism [49], we determined the populations of the spherically symmetrical valence shell (P_{val}) and multipole parameters (P_{lm}) that describe its deformation along with the corresponding expansion and contraction coefficients (k, k') for each atom of complexes **I** and **III**. The multipole decomposition levels were hexadecapole for the tin atom and octupole for all other non-hydrogen atoms. Hydrogen atoms were characterized by one dipole level. The obtained values of P_{val}, P_{lm}, k, and k' were used (but they themselves were not refined) for the multipole refinement of coordinates and thermal parameters of the atoms in complexes **I** and **III** by the experimental sets of reflections ($\sin\theta/\lambda = 0.61$ (**I**) and 0.66 (**III**) Å^{-1}) in the real crystal symmetry.

The topology of the experimental–theoretical function ρ(r) was analyzed using the WINXPRO software [50].

RESULTS AND DISCUSSION

Substituted *o*-benzoquinone ligands **I** and **III** were synthesized according to known procedures [29, 30]. 3,5-Bis(2-phenylpropan-2-yl)-*o*-benzoquinone (L^4) was synthesized by the alkylation of pyrocatechol with α-methylstyrene in the presence of titanium bis(catecholate) followed by the oxidation of pyrocatechol (formed in the first step) with nitric acid (Scheme 1).

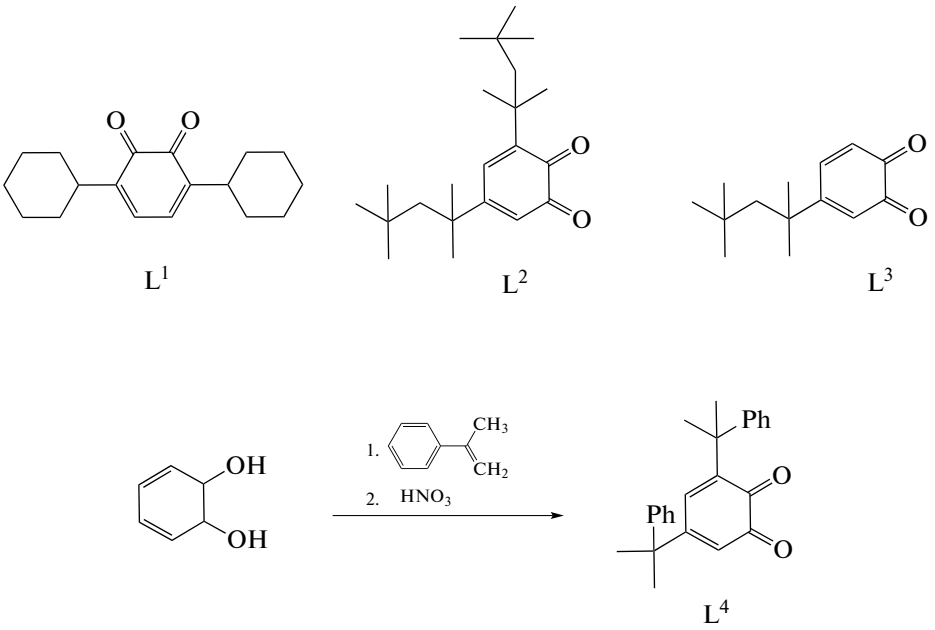

Scheme 1.

The structure of ligand L^4 was confirmed by a complex of physicochemical methods. The IR spectra of benzoquinone L^4 exhibit intense bands at 1640–1700 cm^{-1} characteristic of stretching vibrations of carbonyl groups of sterically shielded benzoquinones. The structure of *o*-quinone L^4 was also confirmed by ^{1}H and ^{13}C NMR spectroscopy data. The ^{1}H NMR spectrum of L^4 is presented by narrow intense signals from the protons of the methyl groups, doublets from the aromatic protons with the constants $^4J_{HH} = 2$ Hz, and multiplets from the protons of the phenyl fragments in positions 3 and 5 of the aromatic ring.

The synthesized substituted *o*-benzoquinones L^1–L^4 readily react with tin dioxanate dichloride in a THF solution (Scheme 2).

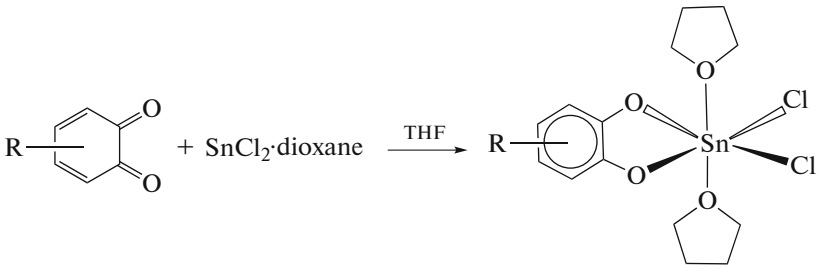

(I)–(IV)

$RCatSnCl_2 \cdot 2THF$

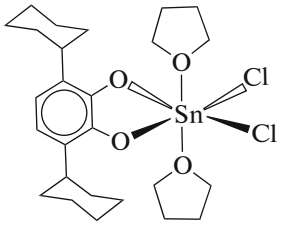

(I)

$(3,6\text{-c-HexCat})SnCl_2 \cdot 2THF$

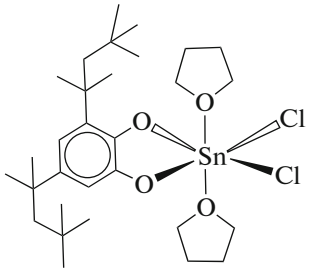

(II)

$(3,5\text{-tret-OctCat})SnCl_2 \cdot 2THF$

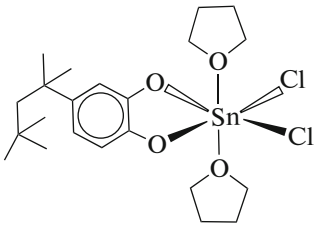

(III)

$(4\text{-tret-OctCat})SnCl_2 \cdot 2THF$

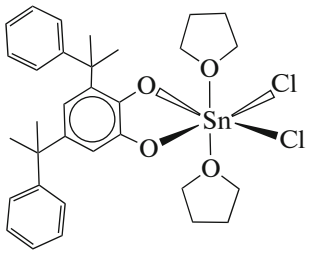

(IV)

$(3,5\text{-C(Me)}_2\text{Ph-Cat})SnCl_2 \cdot 2THF$

Scheme 2.

During the reaction, the low-valent tin(II) atom is oxidized to tin(IV) and *o*-benzoquinone is reduced to the dianionic state to form the corresponding catecholate complexes **I**–**IV** (Scheme 2). The oxidation of Sn(II) to Sn(IV) by *o*-benzoquinone is independent of the molar ratio of the initial reactants and is accompanied by the reduction of one *o*-benzoquinone molecule to catecholate.

The structures of complexes **I**–**IV** were confirmed by various physicochemical methods (IR spectroscopy, ^{1}H NMR, XRD, elemental analysis). The reduction of *o*-benzoquinone is confirmed by the disappearance of the bands corresponding to stretching vibrations of the C=O groups of *o*-benzoquinone in a range of 1650 cm^{-1} in the IR spectra of complexes **I**–**IV** and the presence of absorption bands corresponding to stretching vibrations of C–O ordinary bonds characteristics of the catecholate complexes (1245 cm^{-1}).

All complexes are diamagnetic and have well resolved NMR spectra that also confirm their structures. The ^{1}H NMR spectra of the compounds in a dichloromethane solution contain a set of signals from the protons of the phenyl, methyl, *tert*-octyl, and cyclohexyl groups of the organic ligands in complexes **I**–**IV**. The protons of the aryl ring in the complexes appear in the ^{1}H NMR spectra as signals, whose chemical shifts lie in a range of 6.5–7.1 ppm. In the case of complexes **II** and **IV** based on 3,5-disubstituted *o*-benzoquinone ligands, the signals from the aromatic protons of the catecholate ring are doublets with the constants $^4J_{HH} = 2$ Hz.

The molecular structures of *o*-benzoquinone L^4 and complexes **I** and **III** in the crystalline state were

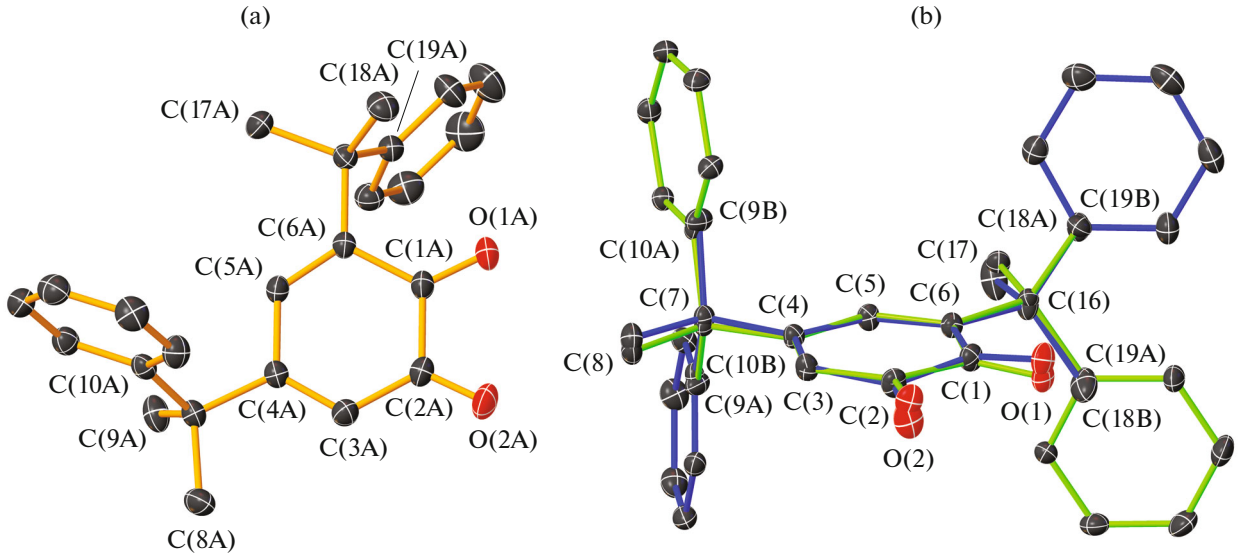

Fig. 1. (a) Structure of molecule **A** in *o*-benzoquinone L^4 (thermal ellipsoids of 30% probability are presented) and (b) the superposition of the structures of molecules **A** and **B** (green and blue bonds, respectively) of compound L^4 with 15% probability thermal ellipsoids of atoms (hydrogen atoms are omitted).

determined by XRD (Figs. 1 and 2). The main bond lengths and angles are given in Table 2.

The asymmetric part of the unit cell of the crystal of *o*-benzoquinone L^4 contains two independent molecules **A** and **B** differed in the positions of the methyl (C(9) and C(18) atoms) and phenyl (C(10) and C(19)) substituents relative to the *o*-benzoquinone plane (Fig. 1b). In molecules **A** and **B**, the methyl groups with C(8) and C(17) lie in the plane of the *o*-benzoquinone cycle. The phenyl groups with the C(10) and C(19) atoms and, correspondingly, the methyl C(9) and C(18) atoms are arranged in the *trans* positions relative to the quinone fragment plane. The structural characteristics of compound L^4 are typical of sterically hindered *o*-benzoquinones (Fig. 1, Table 2). In particular, the C–O distances correspond to double bonds, and the ordinary and double C–C bonds alter in the central six-membered C(1)–C(6) ring. The phenyl groups of the propyl substituents in positions 3 and 5 of the aromatic ring are perpendicular to the *o*-benzoquinone fragment plane due to a necessity to minimize steric interactions. The dihedral angles between them vary in a range of 87.0°–90.0°.

Similarly to L^4, the crystal of compound **III** contains two independent molecules **A** and **B** of the tin(IV) complex differed in the geometry of coordinated THF molecules (Fig. 2c). The tin atoms in complexes **I** and **III** have a distorted octahedral environment (Figs. 2a, 2b). The O(1) and O(2) oxygen atoms of the catecholate fragment and the Cl(1) and Cl(2) chlorine atoms lie in the equatorial plane, whereas the O(3) and O(4) oxygen atoms of two coordinated THF molecules are arranged in the apical positions. The cyclopentadienyl substituents of the catecholate ligand in complex **I** are in the chair conformation. The Sn(1)–O(1,2) bond lengths in complexes **I** and **III** (2.0118(16)–2.0289(14) Å) are close to the sum of covalent radii of oxygen and tin(IV) atoms (2.09 Å) [51] and are rather close to similar bond lengths in various tin(IV) catecholate complexes (1.995(8)–2.079(3) Å) [52–56]. The Sn–Cl bond lengths (2.3426(5)–2.3756(6) Å) in complexes **I** and **III** are typical of Sn^{IV}–Cl bonds (the sum of covalent radii of tin and chlorine atoms is 2.39 Å [51]) and lie in the range of analogous values for the Sn(IV) complexes (2.34–2.46 Å) [57–60]. On the contrary, the Sn–O_{THF} bond lengths for coordinated THF in complexes **I** and **III** exceed the sum of covalent radii of tin and oxygen atoms and demonstrate the donor–acceptor character of the interaction [51, 53]. The C–O bond lengths (1.359(2)–1.375(3) Å) of the catecholate fragment lie in the bond length range for the coordinated dianionic derivatives of the catecholate complexes of diverse metals (from 1.33 to 1.39 Å) [1, 12, 61]. The C–C distances in the aromatic rings of the catecholate ligands are close to analogous values in benzene (1.40 Å).

The experimental–theoretical topology of the electron density was studied for complexes **I** and **III**. For this purpose, we used the aspherical scattering factor of the independent region of the cell (crystalline invariom) that makes it possible to adequately reproduce the topology of the experimental electron density and the energy of intermolecular interactions in the crystal [62, 63]. According to R. Bader's theory [64], all interactions in the coordination sphere of the tin atoms in complexes **I** and **III** are intermediate ($\nabla^2\rho(\mathbf{r}) > 0$, $h_e(\mathbf{r}) < 0$; covalent polar bond; Table 3).

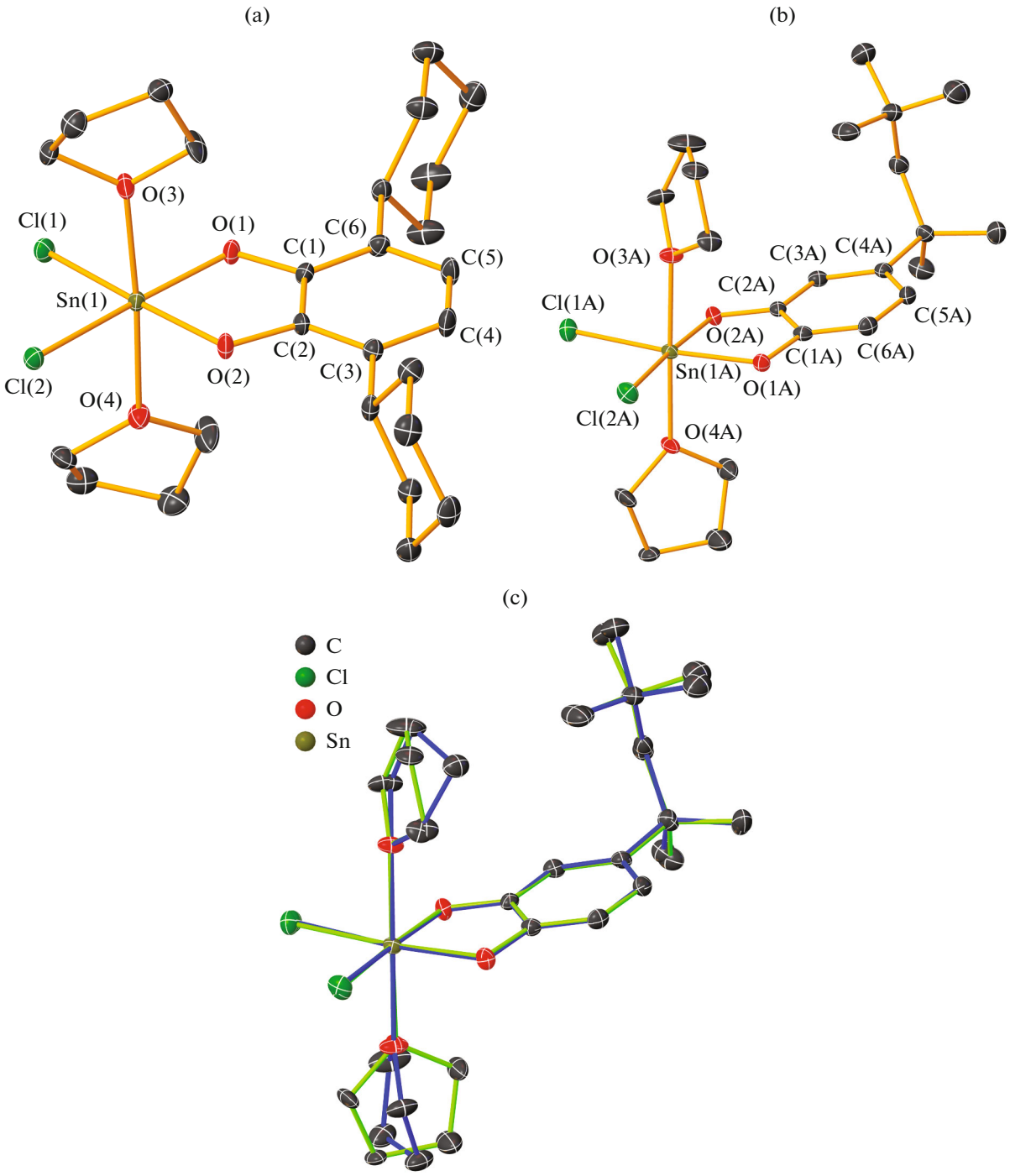

Fig. 2. Molecular structures of complexes (a) **I** and (b) **III** (molecule **A**) and (c) the superposition of the structures of molecules **A** and **B** in complex **III** (green and blue bonds, respectively). Thermal ellipsoids of 50% probability are presented. Hydrogen atoms are omitted.

This agrees with the charge distribution in the coordination sphere of the tin atoms (Table 4). A similar situation is observed in the antimony(V) catecholate and amidophenolate complexes [65, 66]. The total charge on the catecholate center of complex **I** is –0.68 e being somewhat lower than that in complex **III** (–0.76 e).

The oxidation–reduction properties of complexes **I**–**IV** were studied by cyclic voltammetry (CV) in a

Table 2. Selected bond lengths (Å) and angles (deg) in *o*-benzoquinone (L^4) and tin(IV) catecholates (**I**) and (**III**) according to the XRD data

Bond	L^4		**I**	**III**	
	molecule **A**	molecule **B**		molecule **A**	molecule **B**
	d, Å				
Sn(1)–O(1)			2.0163(16)	2.0289(14)	2.0271(14)
Sn(1)–O(2)			2.0118(16)	2.0211(14)	2.0212(14)
Sn(1)–O(3)			2.1694(16)	2.1849(14)	2.1839(14)
Sn(1)–O(4)			2.1891(16)	2.1520(14)	2.1549(14)
Sn(1)–Cl(1)			2.3756(6)	2.3629(6)	2.3620(5)
Sn(1)–Cl(2)			2.3663(6)	2.3453(5)	2.3426(5)
O(1)–C(1)	1.2090(13)	1.2118(14)	1.375(3)	1.361(2)	1.363(2)
O(2)–C(2)	1.2139(13)	1.2099(14)	1.373(3)	1.359(2)	1.360(2)
C(1)–C(6)	1.4859(14)	1.4802(16)	1.393(3)	1.382(3)	1.378(3)
C(1)–C(2)	1.5472(16)	1.5483(18)	1.410(3)	1.414(3)	1.411(3)
C(2)–C(3)	1.4490(15)	1.4502(17)	1.396(3)	1.381(3)	1.373(3)
C(3)–C(4)	1.3419(15)	1.3374(15)	1.396(3)	1.401(3)	1.400(3)
C(4)–C(5)	1.4769(14)	1.4723(15)	1.385(3)	1.393(3)	1.397(3)
C(5)–C(6)	1.3445(14)	1.3393(15)	1.399(3)	1.395(3)	1.394(3)
Angle	ω, deg				
O(1)–Sn(1)–O(2)			83.33(6)	83.12(6)	83.38(6)
Cl(1)–Sn(1)–Cl(2)			95.29(2)	94.61(2)	96.01(2)
O(3)–Sn(1)–O(4)			176.08(6)	178.67(5)	179.21(6)
O(1)–Sn(1)–Cl(1)			90.17(5)	173.15(4)	171.05(4)
O(2)–Sn(1)–Cl(1)			172.20(5)	90.25(4)	87.75(4)
O(1)–Sn(1)–Cl(2)			174.07(5)	92.00(4)	92.83(4)
O(2)–Sn(1)–Cl(2)			91.39(5)	175.09(4)	175.91(4)

Table 3. Selected experimental–theoretical topological parameters of the electron density in the coordination sphere of the tin atom*

Bond	$v(\mathbf{r})$, au	$\rho(\mathbf{r})$, au	$\nabla^2\rho(\mathbf{r})$, au	$h_e(\mathbf{r})$, au
		V		
Sn(1)–O(1)	–0.178	0.109	0.408	–0.038
Sn(1)–O(2)	–0.180	0.110	0.411	–0.038
Sn(1)–O(3)	–0.098	0.076	0.239	–0.019
Sn(1)–O(4)	–0.092	0.073	0.223	–0.018
Sn(1)–Cl(1)	–0.099	0.081	0.145	–0.031
Sn(1)–Cl(2)	–0.100	0.081	0.150	–0.031
		VII		
Sn(1A)–O(1A)	–0.167	0.105	0.394	–0.034
Sn(1A)–O(2A)	–0.172	0.107	0.406	–0.035
Sn(1A)–O(3A)	–0.093	0.073	0.230	–0.017
Sn(1A)–O(4A)	–0.103	0.078	0.254	–0.020
Sn(1A)–Cl(1A)	–0.103	0.083	0.153	–0.032
Sn(1A)–Cl(2A)	–0.107	0.085	0.161	–0.034

* Potential energy density ($v(\mathbf{r})$), electron density ($\rho(\mathbf{r})$), electron density Laplacian ($\nabla^2\rho(\mathbf{r})$), and electron energy density ($h_e(\mathbf{r})$) at the critical points (3, –1).

Table 4. Atomic charges (q/e) in the coordination sphere of tin calculated experimentally–theoretically

Complex	q(Sn(1))	q(O(1))	q(O(2))	q(O(3))	q(O(4))	q(Cl(1))	q(Cl(2))
I	1.89	–0.95	–0.96	–0.86	–0.85	–0.58	–0.56
III*	1.92	–0.96	–0.96	–0.84	–0.88	–0.56	–0.56

* The charges are presented for one independent molecule (A).

Table 5. Electrochemical potentials (V) of the oxidation of complexes **I**–**IV** (298 K, Ag/AgCl/KCl, CH_2Cl_2, $c = 1 \times 10^{-3}$ M, 0.2 M [n-Bu_4N]ClO_4, $V = 0.2$ V/s, Ar)

Complexes	E_p, V*
I	1.24
II	1.14
III	1.22
IV	1.20

* E_p is the peak potential for the irreversible process.

dichloromethane solution under an argon atmosphere (Fig. 3, Table 5). The CV curves typical of these compounds in a range of 0.2–1.6 V are shown in Fig. 3.

The cyclic voltammograms of tin(IV) complexes **I**–**IV** demonstrate one irreversible step of electrochemical oxidation in the range from 0.95 to 1.30 V corresponding to the oxidation of the catecholate center. It should be mentioned that the charges on the catecholate centers in compounds **I** (–0.68 e) and **III** (–0.76 e) correlate with the electrochemical oxidation potential (Table 5). The higher the negative charge, the lower the electrochemical oxidation potential. This confirms that the use of crystalline invarioms is correct for studying the electron density topology.

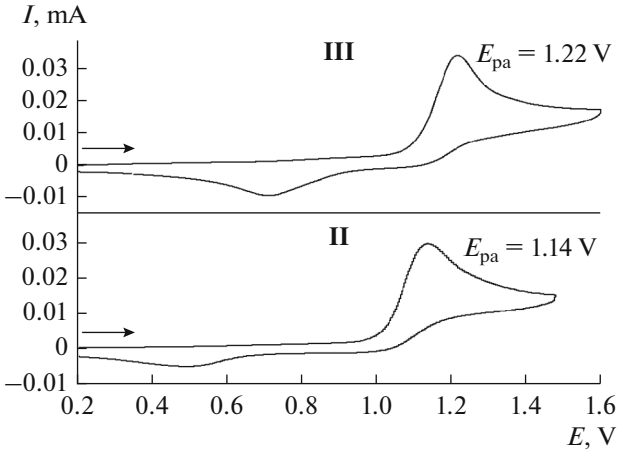

Fig. 3. CV curves for complexes **II** and **III** (glassy carbon electrode, Ag/AgCl/KCl, 0.2 M [n-Bu_4N]ClO_4, CH_2Cl_2, $c = 2 \times 10^{-3}$ mol/L, $V = 0.2$ V/s, Ar).

Thus, sterically hindered o-benzoquinone (L^4) and related complex (3,5-C(Me)$_2$Ph-Cat)$SnCl_2$·2THF (**IV**), as well as the series of monocatecholate tin(IV) complexes with substituted o-benzoquinone ligands were synthesized. The molecular structures of ligand L^4 and two complexes (3,6-c-HexCat)$SnCl_2$·2THF (**I**) and (4-*tret*-OctCat)$SnCl_2$·2THF (**III**) in the crystalline form were determined by XRD. The oxidation–reduction properties of the synthesized compounds were studied by cyclic voltammetry. The electrochemical oxidation of the complexes was shown to occur in a range of 1.14–1.24 V as a one-step process involving the catecholate center.

ACKNOWLEDGMENTS

The work was carried out using the equipment of the Center for Collective Use "Analytical Center of Institute of Organometallic Chemistry of Russian Academy of Sciences" and supported by the project "Provision of Development of Material Technical Infrastructure of Centers for Collective Use of Scientific Equipment" (unique identifier RF–2296.61321X0017, agreement no. 075-15-2021-670).

FUNDING

This work was supported by the Council on Grants of the President of the Russian Federation for state support of young Russian scientists and leading scientific schools of the Russian Federation (project no. NSh-403.2022.1.3). The study of the experimental–theoretical electron density was supported by the Russian Science Foundation, project no. 21-13-00336.

CONFLICT OF INTEREST

The authors of this work declare that they have no conflicts of interest.

REFERENCES

1. Pierpont, C., *Coord. Chem. Rev.*, 2001, vols. 219–221, p. 415.
2. Kaim, W., *Inorg. Chem.*, 2011, vol. 50, p. 9752.
3. Mao, G., Song, Y., Hao, T., et al., *Chin. Sci. Bull.*, 2014, vol. 59, p. 2936.
4. Starikova, A.A. and Minkin, V.I., *Russ. Chem. Rev.*, 2018, vol. 87, p. 1049.
5. Fomenko, I.S. and Gushchin, A.L., *Russ. Chem. Rev.*, 2020, vol. 89, p. 966.

6. Broere, D.L., Plessius, R., and Van der Vlugt, J.I., *Chem. Soc. Rev.*, 2015, vol. 44, p. 6886.
7. Luca, O.R. and Crabtree, R.H., *Chem. Soc. Rev.*, 2013, vol. 42, p. 1440.
8. Baryshnikova, S.V. and Poddel'sky, A.I., *Molecules*, 2022, vol. 27, p. 3928.
9. Ershova, I.V., Piskunov, A.V., and Cherkasov, V.K., *Russ. Chem. Rev.,* 2020, vol. 89, p. 1157.
10. Pashanova, K.I., Poddel'sky, A.I., and Piskunov, A.V., *Coord. Chem. Rev.*, 2022, vol. 459, p. 214399.
11. Zanello, P. and Corsini, M., *Coord. Chem. Rev.*, 2006, vol. 250, p. 2000.
12. Poddel'skii, A.I., Abakumov, G.A., Bubnov, M.P., Cherkasov, V.K., and Abakumova, L.G., *Izv. Akad. Nauk., Ser. Khim.*, 2004, no. 6, p. 1142.
13. Abakumov, G.A. and Nevodchikov, V.I., *Dokl. Akad Nauk SSSR*, 1982, vol. 266, no. 6, p. 1407.
14. Lange, C.W., Foldeaki, M., Nevodchikov, V.I., et al., *J. Am. Chem. Soc.*, 1992, vol. 114, p. 4220.
15. Jung, O.-S. and Pierpont, C.G., *J. Am. Chem. Soc.*, 1994, vol. 116, p. 2229.
16. Nevodchikov, V.I., Abakumov, G.A., Cherkasov, V.K., and Razuvaev, G.A., *J. Organomet. Chem.*, 1981, vol. 214, p. 119.
17. Pierpont, C.G. and Buchanan, R.M., *Coord. Chem. Rev.*, 1981, vol. 38, p. 45.
18. Poddel'sky, A.I., Cherkasov, V.K., and Abakumov, G.A., *Coord. Chem. Rev.*, 2009, vol. 253, p. 291.
19. Abakumov, G.A., Poddel'sky, A.I., Grunova, E.V., et al., *Angew. Chem.*, 2005, vol. 117, p. 2827.
20. Cherkasov, V.K., Abakumov, G.A., Grunova, E.V., et al., *Chem.-Eur. J.*, 2006, vol. 12, p. 3916.
21. Piskunov, A.V., Ershova, I.V., Fukin, G.K., and Shavyrin, A.S., *Inorg. Chem. Commun.*, 2013, vol. 38, no. 12, p. 127.
22. Piskunov, A.V., Piskunova, M.S., and Chegerev, M.G., *Russ. Chem. Bull.*, 2014, no. 4, p. 912.
23. Fedushkin, I.L., Dodonov, V.A., Skatova, A.A., et al., *Chem.-Eur. J.*, 2018, vol. 24, no. 8, p. 1877.
24. Fedushkin, I.L., Nikipelov, A.S., Morozov, A.G., et al., *Chem.-Eur. J.*, 2012, vol. 18, p. 255.
25. Ilyakina, E.V., Poddel'sky, A.I., Cherkasov, V.K., and Abakumov, G.A., *Mendeleev Commun.*, 2012, vol. 22, p. 208.
26. Ilyakina, E.V., Poddel'sky, A.I., and Piskunov, A.V., et al., *Inorg. Chim. Acta*, 2013, vol. 394, p. 282.
27. Gordon, A. and Ford, R., *The Chemist's Companion: A Handbook of Practical Data, Techniques, and References*, New York: Wiley, 1972.
28. Reichhardt, C., *Solvents and Solvent Effects in Organic Chemistry*, Weinheim: VCH, 1988.
29. Kocherova, T.N., Druzhkov, N.O., Mart'yanov, K.A., et al., *Russ. Chem. Bull.*, 2020, vol. 69, no. 12, p. 2383.
30. Kocherova, T.N., Druzhkov, N.O., Arsen'ev, M.V., et al., *Russ. Chem. Bull.*, 2023, vol. 72, no. 5, p. 1192.
31. *Data Collection, Reduction and Correction Program. CrysAlisPro 1.171.38.46—Software Package*, Rigaku OD, 2015.
32. *APEX4. Bruker Molecular Analysis Research Tool. Version 2021.4-0*, Madison: Bruker AXS Inc., 2021.
33. *SAINT Data Reduction and Correction Program. Version 8.40B*, Madison: Bruker AXS, 2019.
34. Krause, L., Herbst-Irmer, R., Sheldrick, G.M., and Stalke, D., *J. Appl. Crystallogr.*, 2015, vol. 48, p. 3.
35. Sheldrick, G., *Acta Crystallogr., Sect. A: Found Adv.*, 2015, vol. 71, p. 3.
36. Sheldrick, G.M., *SHELXTL. Version 6.14. Structure Determination Software Suite*, Madison: Bruker AXS, 2003.
37. Sheldrick, G., *Acta Crystallogr., Sect. C: Struct. Chem.*, 2015, vol. 71, p. 3.
38. *SCALE3 ABSPACK: Empirical absorption correction. CrysAlisPro 1.171.38.46—Software Package*, Rigaku OD, 2015.
39. *SADABS. Version 2016/2. Bruker/Siemens Area Detector Absorption Correction Program*, Madison: Bruker AXS, 2016.
40. Becke, A.D., *J. Chem. Phys.*, 1993, vol. 98, p. 5648.
41. Lee, C., Yang, W., and Parr, R.G., *Phys. Rev. B*, 1988, vol. 37, p. 785.
42. Dovesi, R., Erba, A., Orlando, R., Zicovich-Wilson, C.M., Civalleri, B., Maschio, L., Rerat, M., Casassa, S., Baima, J., Salustro, S., and Kirtman, B., *WIREs Comput. Mol. Sci.*, 2018, vol. 8, p. e1360.
43. Godbout, N., Salahub, D.R., Andzelm, J., and Wimmer, E., *Can. J. Chem.*, 1992, vol. 70, p. 560.
44. Pritchard, B.P., Altarawy, D., Didier, B., et al., *J. Chem. Inf. Model*, 2019, vol. 59, p. 4814.
45. Feller, D., *J. Comput. Chem.*, 1996, vol. 17, p. 1571.
46. Schuchardt, K.L., Didier, B.T., Elsethagen, T., et al., *J. Chem. Inf. Model*, 2007, vol. 47, no. 3, p. 1045.
47. Spek, A.L., *Acta Crystallogr., Sect. C: Struct. Chem.*, 2015, vol. 71, p. 9.
48. Jelsch, C., Guillot, B., Lagoutte, A., and Lecomte, C., *J. Appl. Crystallogr.*, 2005, vol. 38, p. 38.
49. Hansen, N.K. and Coppens, P., *Acta Crystallogr., Sect. A: Cryst. Phys., Diffr., Theor. Gen. Crystallogr.*, 1978, vol. 34, p. 909.
50. Stash, A.I. and Tsirelson, V.G., *J. Appl. Crystallogr.*, 2014, vol. 47, p. 2086.
51. Batsanov, S., *Russ. J. Inorg. Chem.*, 1991, vol. 36, p. 1694.
52. Baryshnikova, S.V., Poddel'sky, A.I., Bellan, E.V., et al., *Inorg. Chem.*, 2020, vol. 59, p. 6774.
53. Lado, A.V., Poddel'sky, A.I., Piskunov, A.V., et al., *Inorg. Chim. Acta*, 2005, vol. 358, p. 4443.
54. Piskunov, A.V., Lado, A.V., Ilyakina, E.V., et al., *J. Organomet. Chem.*, 2008, vol. 693, p. 128.
55. Turek, J., Kampová, H., Padelkova, Z., and Ruzicka, A., *J. Organomet. Chem.*, 2013, vols. 745–746, p. 25.
56. Annan, T.A., McGarvey, B.R., Ozarowski, A., et al., *Dalton Trans.*, 1989, vol. 3, p. 439.
57. Zubieta, J.A. and Zuckerman, J.J., *Prog. Inorg. Chem.*, New York: Wiley, 1978, vol. 24, p. 251.
58. Archer, S.J., Koch, K.R., and Schmidt, S., *Inorg. Chim. Acta*, 1987, vol. 126, p. 209.

59. Baryshnikova, S.V., Bellan, E.V., Poddel'sky, A.I., et al., *Eur. J. Inorg. Chem*, 2016, no. 33, p. 5230.
60. Ilyakina, E.V., Poddel'sky, A.I., Fukin, G.K., et al., *Inorg. Chem.*, 2013, vol. 52, p. 5284.
61. Brown, S.N., *Inorg. Chem.*, 2012, vol. 51, p. 1251.
62. Fukin, G.K. and Cherkasov, A.V., *Mendeleev Commun.*, 2021, vol. 31, p. 182.
63. Pochekutova, T.S., Fukin, G.K., Baranov, E.V., et al., *Inorg. Chim. Acta*, 2022, vol. 531, p. 120734.
64. Bader, R.F.W., *Atoms in Molecules: A Quantum Theory.* Oxford: Oxford Univ., 1990.
65. Fukin, G.K., Baranov, E.V., Jelsch, C., et al., *J. Phys. Chem. A*, 2011, vol. 115, p. 8271.
66. Fukin, G.K., Samsonov, M.A., Baranov, E.V., et al., *Russ. Chem. Bull.*, 2016, no. 1, p. 54.

Translated by E. Yablonskaya